DOI: 10.21062/mft.2025.034 http://www.journalmt.com

Analysis and Optimization of Horizontal Centrifugal Casting Process for Thick Walled Alloy Layers in Tilting Pad Bearings

Ye Jun (0009-0002-6988-9293)[1,2], Jin Jing (0009-0004-0512-4421)[4], Wang Guobiao (0000-0003-2076-748X)[1*], Xu Zhaohui (0009-0002-2256-2576)[3], Guo Huangsha (0009-0006-3222-5871)[3]
[1]School of Mechanical Engineering, Tianjin University. No. 135, Yaguan Road, Jinnan District, Tianjin, China. E-mail: 20150009@zjipc.edu.cn
[2]School of Electromechanical Engineering, Zhejiang Industry Polytechnic College, No. 151, Qutun, Yuecheng District, Shaoxing City, Zhejiang Province, China.
[3]Zhejiang Shenfa Bearing Co., Ltd. No. 59, Kuahu Road, Chengxi Development Zone, Zhuji City, Zhejiang Province, China. E-mail: shenfagroup@hotmail.com
[4]Rail Transit Department, Zhejiang Institute of Communications, No. 1515 Moganshan Road, Yuhang District, Hangzhou City, Zhejiang Province, China.

The optimization of process parameters plays a critical role in controlling temperature and velocity fields during centrifugal casting, which is essential for mitigating shrinkage porosity defects caused by uneven cooling in thick walled bearing alloy layers. In this study, two sequential numerical models were developed using ProCAST software to simulate gravity filling and centrifugal solidification stages. The effects of key parameters, including inlet cross-sectional area and centrifugal rotational speed, on flow field characteristics were systematically analyzed. By using an orthogonal experimental design, we determined the optimal parameters: a melt temperature of 440 °C for the Babbitt alloy, an initial temperature of 280 °C for the bearing blank, a filling inlet diameter of 16 mm, and a rotational speed of 340 r/min. Bearing alloy layers manufactured according to these optimized parameters exhibit no evident shrinkage or cracks on their surfaces. The high quality finished products meet the design requirements, thereby validating the accuracy of the numerical simulation.

Keywords: Centrifugal Casting, ProCAST, Shrinkage Porosity, Orthogonal Experiment

1 Introduction

The tilting-pad bearing, a specialized type of plain bearing, consists of multiple independently tilting pads capable of free rotation around their respective fulcrums. Widely applied in supporting large steam turbines and nuclear power main pumps[1,2], it requires a Babbitt alloy layer of appropriate thickness cast onto the inside tilting-pad surface to enhance performance and service life. Horizontal centrifugal casting is extensively employed in the fabrication of tilting-pad bearing alloy layers due to its ability to rapidly execute the casting process, ensure uniform wall thickness distribution crucial for performance, and effectively reduce casting defects like shrinkage porosity and poor metallurgical bonding [3].

More and more scholars have been conducting research on the optimization of casting process parameters[4, 5]. Ran X [6] employed the Procast simulation method to study the filling process of the cross runner casting system for large ring titanium alloy castings. Wang X. et al. [7,8] established a numerical model for centrifugal casting of very large cylindrical liner, and studied the effects of centrifugal speed and filling time on the filling and solidification process. Xin, M. et al. [9] prepared large near-net-shaped aluminum alloy pipes through the centrifugal casting method and established a heat flow simulation model by utilizing Procast. They conducted an in-depth study on the process parameters and solidification behavior, and ultimately determined the optimal casting temperature and centrifugal speed. Dong Q et al. [10] constructed a continuous flow model for horizontal centrifugal casting and investigated the impacts of diverse rotational speeds, pouring velocities, and cooling techniques on the temperature field during the filling and solidification of the Babbitt lining. Yang Y et al. [11] adopted orthogonal experimental design to optimize the process parameters (speed, mold preheating temperature, pouring temperature) of vertical centrifugal casting, so as to reduce defects in Ti-6Al-4V (TC4) alloy wheels during vertical centrifugal casting. In order to improve the quality of impeller centrifugal castings, Yu-Chol K et al. [12] made inclined arrangement of impeller shell, optimized the gate/riser system, and further analyzed the solidification behavior of molten metal by using ProCAST. Mazloum K et al. [13] used finite element analysis software to study the influence of parameters such as length-diameter ratio, pouring temperature and mold speed on casting quality, so as to determine

the best casting conditions. Shi J [14] analyzed the mechanical model of the filling process of vertical centrifugal casting for thin-wall components, established a solver and optimized the casting process.

During the centrifugal casting process, the centrifugal force acting on the flowing metal alloy is directly proportional to the product of the rotational speed squared and the radius. In the production scenarios of first tier enterprises, due to the large radius, a significant amount of casting metal liquid, complex fluid motion, and uneven cooling in the manufacturing of these large wall thickness tilting pad bearing alloy castings, more prominent shrinkage and porosity issues often occur. Therefore, it is extremely essential to conduct a comprehensive analysis and optimization of the horizontal centrifugal casting process for the thick walled alloy layers in tilting pad bearings. This analysis and optimization are crucial for enhancing the quality of the castings and ensuring the reliable operation of tilting pad bearings in practical applications.

In this paper, the numerical simulation models of gravity and centrifugal casting were established, the influence mechanism of different process parameters (including centrifugal speed, inlet area, etc.) on the flow field and temperature field was studied, and the optimal process parameters are determined through orthogonal tests, and finally the experimental verification and analysis were carried out.

2 Casting Model and Materials

The tilting pad bearing product (model SH-08J) used for steam turbine transmission and sourced from an enterprise in Zhuji City, Zhejiang Province is the focus of the present study. The bearing's main structure consists of a plurality of tilting pads arranged in a circular formation. To simplify the numerical simulation process and avoid unnecessary grid division, the solid model of the tilting pad bearing was simplified. The main simplification methods involve omitting the oil groove, oil inlet hole, oil outlet hole, and bolt connection holes, and simplifying the centrifugally cast alloy layer product into a sleeve type part (as depicted in Fig. 1). The specific parameters are as follows: the outer diameter of the bearing shell is 1060 mm, the inner diameter is 560 mm, the height is 450 mm, and the thickness of the alloy layer is 15 mm.

The centrifugal casting principle of the large wall thickness tilting pad bearing is shown in Fig. 2. The bearing blank is securely clamped between two rotating discs. The rotation of the bearing blank is induced by the clamping frictional force exerted by the rotating discs. The high temperature Babbitt alloy melt is then introduced into the bearing blank through the left hand runner. Under the influence of centrifugal force, the poured Babbitt metal uniformly distributes and flows along the inner wall of the bearing blank body. Eventually, following the cooling process, it solidifies to form the alloy layer of the tilting pad bearing, which is crucial for the bearing's performance and functionality.

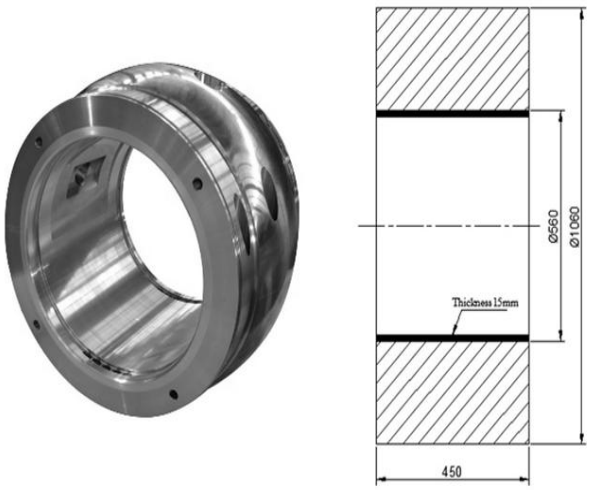

Fig. 1 *Tilting pad bearing and casting dimension of steam turbine*

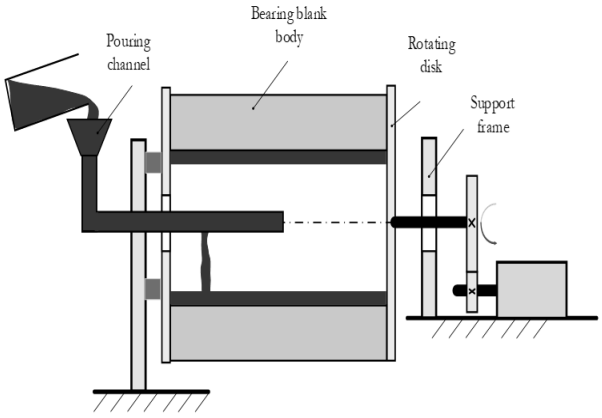

Fig. 2 *Centrifugal casting of tilting-pad bearing*

The alloy layer of the tilting pad bearing must possess excellent wear resistance and stability. Tin-base Babbitt metal is a commonly used material for the alloy layer. Among these materials, ZSnSb11Cu6 is the most frequently used one, and its specific chemical composition is presented in Tab. 1. Since the material library of Procast software does not include tin based materials, in order to obtain the properties of ZSnSb11Cu6 material, it is necessary to input its chemical composition into JMatPro material performance simulation software for calculation [15]. Subsequently, the data is converted into a format readable by Procast for subsequent Procast simulation tests. Fig. 3 below illustrates the Newtonian viscosity curv of the ZSnSb11Cu6 . Additionally, the liquidus temperature of this material is 364 °C, and the solidus temperature is 211 °C.

Tab. 1 *Chemical composition of ZSnSb11Cu6*

	Chemical composition (mass fraction)/%					
ZSnSb11Cu6	Sn	Cu	Pb	Bi	Sb	the rest
	The rest	6	0.35	0.03	10.0~12.0	0.1

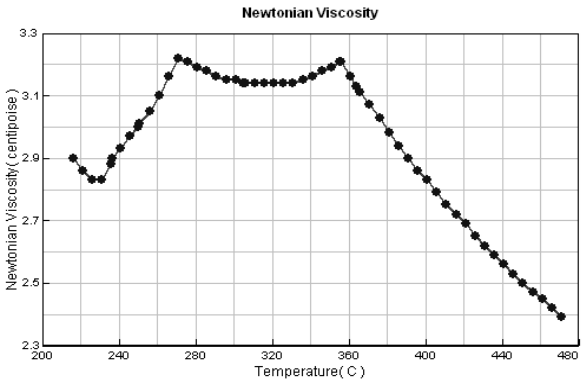

Fig. 3 *The Newtonian viscosity curv of the ZSnSb11Cu6*

3 Mathematical model

In modern casting technology, the process from molten alloy flow through the gate into the mold cavity until final solidification completion primarily consists of two critical stages: filling and solidification. These stages directly determine the quality of the final casting product. The high temperature alloy melt in the cavity undergoes a three-dimensional continuous flow process, which can be characterized as an incompressible viscous fluid with a free surface. At the solid mold walls, the fluid velocity matches the wall velocity through implementation of the no-slip boundary condition. It is assumed that the high temperature alloy liquid pouring rate from the runner remains constant throughout the centrifugal casting process and that the high temperature alloy liquid will achieve the same rotational speed as the rotating bearing blank after the filling process. Therefore, the whole process of high temperature alloy liquid filling cavity conforms to the mass continuity equation [16].

$$\frac{\partial \rho}{\partial t}+\frac{\partial(\rho u)}{\partial x}+\frac{\partial(\rho v)}{\partial y}+\frac{\partial(\rho \omega)}{\partial z}=0 \tag{1}$$

Where:

u,v,w …The velocity vector of superalloy in x,y,z direction[m/s]**;**

ρ …The density of the metal fluid[kg/m^3].

Moreover, during the filling process, the molten high temperature alloy adheres to the momentum conservation principle. Once the initial and boundary conditions are defined, the subsequent Navier-Stokes(N-S) equations are fulfilled.

$$\begin{cases}\rho(\dfrac{\partial u}{\partial t}+u\dfrac{\partial u}{\partial x}+v\dfrac{\partial u}{\partial y}+w\dfrac{\partial u}{\partial z})=-\dfrac{\partial p}{\partial x}+\rho g_x+\mu\nabla^2 u\\ \rho(\dfrac{\partial v}{\partial t}+u\dfrac{\partial v}{\partial x}+v\dfrac{\partial v}{\partial y}+w\dfrac{\partial v}{\partial z})=-\dfrac{\partial p}{\partial y}+\rho g_y+\mu\nabla^2 v\\ \rho(\dfrac{\partial w}{\partial t}+u\dfrac{\partial w}{\partial x}+v\dfrac{\partial w}{\partial y}+w\dfrac{\partial w}{\partial z})=-\dfrac{\partial p}{\partial z}+\rho g_z+\mu\nabla^2 w\end{cases} \tag{2}$$

Where:

p …The pressure inside the centrifugal casting system [Pa];

g_x,g_y,g_z …The component of acceleration in x,y,z direction [m/s^2];

μ …The kinematic viscosity of the high temperature alloy liquid [m^2/s];

∇^2 …The Laplace operator.

The solidification process of the molten high temperature alloy is a complex phenomenon that encompasses numerous scientific principles, including those related to thermodynamics, dynamics, and microstructure evolution. From a thermodynamic perspective, during the solidification of the high temperature alloy liquid, heat transfer predominantly occurs through heat conduction, heat convection, and heat radiation. This process principally adheres to the energy conservation equation [17].

$$\rho c_p\frac{\partial T}{\partial t}=\frac{\partial}{\partial x}(\lambda\frac{\partial T}{\partial x})+\frac{\partial}{\partial y}(\lambda\frac{\partial T}{\partial y})+\frac{\partial}{\partial z}(\lambda\frac{\partial T}{\partial z})+Q \tag{3}$$

Where:

T …The temperature of high-temperature fluid [K];

λ …The thermal conductivity of molten high temperature alloy [W/(m.K)];

Q …The heat source phase, $Q=\rho \mathrm{L}\dfrac{\partial f_s}{\partial T}$;

c_p …The specific heat capacity of molten high temperature alloy under constant pressure [J/(kg.K)].

4 Three dimensional Model and Process Parameters

In the process of horizontal centrifugal casting, firstly, the high temperature liquid flows into the inside of the embryo under the action of gravity. After contacting the inner surface of the embryo, it starts to have centrifugal force and Coriolis force under the action of centrifugal force. For the numerical simulation software on the market, the interface type of the same material is "EQUIV", which will be considered as a whole. Centrifugally cast runner and fill cavities are of the same material. In this horizontal centrifugal casting model of alloy layer for large wall thickness tilting-pad bearing, the runner and the filling cavity are made of the same material, so they will be considered as the same whole with centrifugal force, however, this is inconsistent with the actual situation. In this paper, the whole centrifugal casting process is divided into two parts: one is gravity casting model and the other is centrifugal casting model. The gravity casting model is mainly used to obtain the initial conditions of superalloy liquid at the inlet of centrifugal casting model, mainly including the entry speed, time and initial position.

Fig. 4 (a) below illustrates the gravity casting model. The key components involved in the gravity model stage are the runner and the bearing alloy layer cavity. Hence, in this study, the runner and the alloy layer cavity are connected by a square shaped cavity and regarded as an integrated component. In this model, the pouring inlet plane of the molten high temperature alloy is 150 mm away from the center of the rotating circle. The integral runner is horizontally arranged with a pipe diameter of 40 mm, and two 8 mm holes are drilled on the horizontal pipe, 90 mm from the left and right end faces respectively. The molten high temperature alloy enters the interior of the bearing blank through the holes at both ends of a horizontally placed bend under the influence of gravity. In the numerical model, the grid size of the runner is set to 2 mm, and the grid size of the casting alloy layer cavity is set to 10 mm, resulting in approximately 1.96 million grids.

In accordance with the requirements of gravity casting, a circular region with a radius of 10 mm is designated as the casting inlet of the model, and a mass flow rate of 100 kg/min is specified. As can be observed from the gravity phase simulation presented in Fig. 4 (b) (where the -Y direction represents the gravity direction), under steady flow conditions, the metal solution passing through the two apertures exhibits a larger volume in the upper part and a smaller volume in the lower part. This study takes the horizontal pipeline fully filled with superalloy as input parameters for subsequent centrifugal casting. At this stage, the alloy layer reaches a position 15 mm above the bottom, exhibiting a circular cross-section with a diameter 2.3 times that of the pipeline outlet, while maintaining a flow velocity of 2.28 m/s. Additionally, the horizontal pipeline is equipped with a mechanical valve device that simultaneously opens the two inlet ports, ensuring no time lag occurs when high-temperature liquid from both ends enters the centrifugal casting chamber.

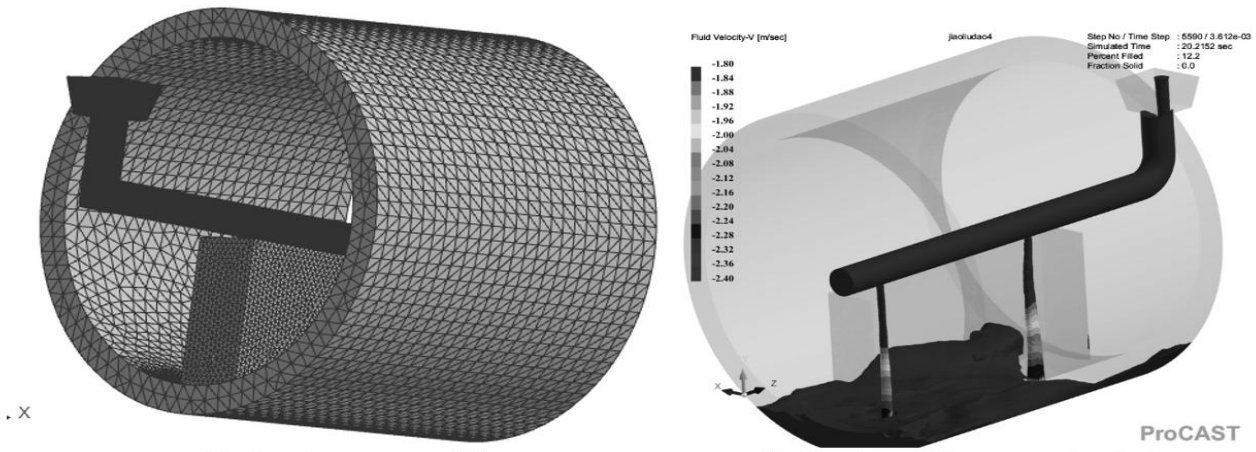

(a) Gravity stage model (b) Gravity casting stage simulation

Fig. 4 *Gravity casting stage simulation of the tilting pad*

Fig. 5 illustrates a centrifugal casting model. This model consists of left and right circular plates, a bearing blank, and a casting alloy layer. Consequently, the centrifugal casting model was constructed using Creo 3D software and then imported into Procast software in igs format. The grid size of the casting alloy layer was set to 4 mm, and the grid size of the two side plates and the blank was set to 20 mm, resulting in approximately 5.49 million grids. The bearing blank is fabricated from No. 25 steel, while the disks on both sides are made of No. 45 steel.

During the simulation of the centrifugal casting model, the key process parameters comprise centrifugal speed, initial temperature of the blank, casting temperature, casting inlet area, inlet velocity, and other relevant parameters [18,19]. The centrifugal casting

rotation speed is mainly determined according to the following formula.

$$n = 29.9\sqrt{G/R} \quad (4)$$

Where:

G …Brozoff gravity coefficient;

R …The inner surface radius of the casting [m].

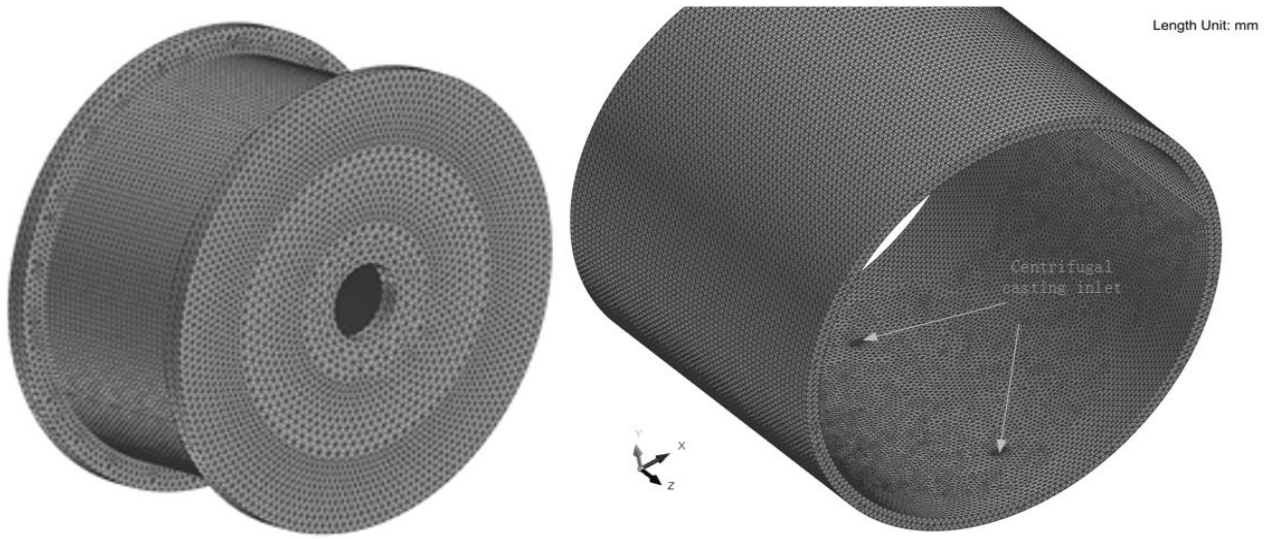

Fig. 5 *Centrifugal Casting stage simulation of the tilting pad bearing*

In this study, the value of G is set as 45, and the inner surface radius of the casting is 0.28 m. As derived from formula (4), the calculated centrifugal speed of the bearing blank is 397.05 r/min, which is then rounded up to 380 r/min. Moreover, the other casting process parameters are configured as follows: the temperature of the Babbitt metal is set at 420 °C, the pre heating temperature of the bearing blank is 300 °C, the casting filling rate of the bearing alloy layer model is 51.4%. Due to the centrifugal force-induced stress state in the molten high temperature alloy, the heat transfer coefficient between the bearing blank body and the casting components is consequently elevated compared to other regions. This interfacial coefficient is assigned a value of 3200 W/(m²·K), while the heat transfer coefficient between unstressed components is specified as 2000 W/(m²·K). Furthermore, water cooling is implemented on the external surface of the bearing blank, whereas convective air cooling is employed for the remaining structural elements.

5 Simulation test and analysis

5.1 Influence of different inlet area on casting filling

In centrifugal casting filling, there is the following relationship among filling time, flow rate and inlet area.

$$v_a = \frac{VF_l}{100S_A F_t} \quad (5)$$

Where:

v_a …The flow velocity at the inlet [m/s];

V …The volume to be filled [m³];

F_l …The filling rate of the entire cavity volume [%];

S_A …The area of the cast entry [m²];

F_t …The filling time of the monolithic casting [s].

Based on the aforementioned 3D model and process parameters, in this study, the runner height of the gravity casting model is fixed. Consequently, the inlet velocity of the centrifugal casting model is also determined. Moreover, the filling rate of the centrifugal casting model remains constant. As a result, the filling time of the model is solely related to the area of the casting inlet. In order to study the influence of different filling times on the castings, under the condition that other initial conditions remain unchanged, two entrance areas of the flow channel were set as circular regions with radii of 6mm, 9mm and 12mm respectively.

Fig. 6 depicts the flow field of centrifugal casting at 10% filling for different runner areas. When the molten high temperature alloy enters the cavity, it spreads towards both end faces, creating a void region in the middle. This area will be filled with the molten high temperature alloy after one rotation, and there is a temperature difference between the newly entered alloy and that in this area. From the perspective of the centrifugal casting process, the smaller the area of this hollow region is, the more favorable it is for the casting of the alloy layer. Compared to the 12 mm casting model, the casting processes with radii of 6 mm and 9 mm cause the metal melts from the two runner channels to converge for centrifugal motion, taking 4.67 s and 2.01 s respectively. Among the three models with different filling times, in the flow field

with a filling inlet radius of 6 mm, there is more accumulation of the molten high temperature alloy at the bottom. This is not conducive to the final uniform flow of the entire flow field and may lead to the problem of uneven wall thickness of the bearing Babbitt layer.

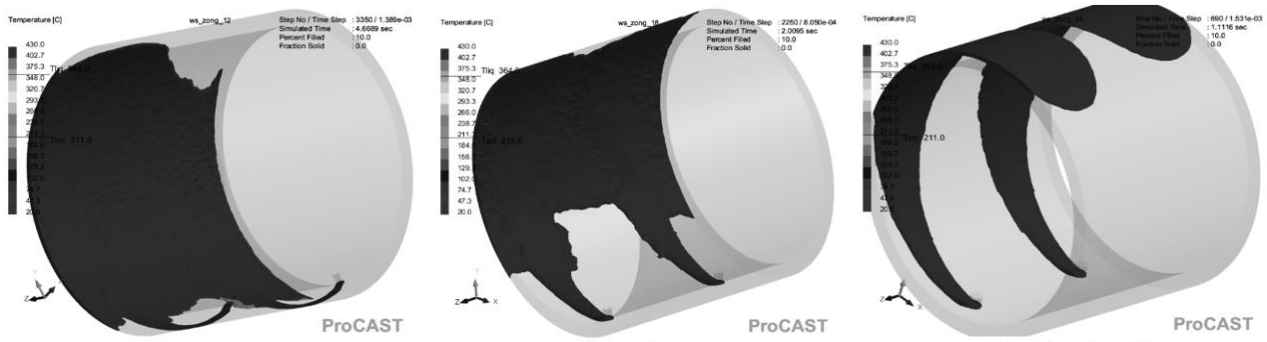

a) Inlet radius 6mm b) Inlet radius 9mm c) Inlet radius 12mm

Fig. 6 *Filling inlets of different areas (filling 10%)*

As can be inferred from the above analysis, when the inlet area is too small, an insufficient amount of molten high temperature alloy will enter the cavity. In addition, there will not be sufficient frictional force to propel the molten alloy to rotate, causing it to accumulate at the bottom. Conversely, if the inlet area is too large, the two inlets will function independently as runners, leading to an unfilled region between the two runners. Therefore, a filling inlet radius of 9 mm is preliminarily chosen.

5.2 Effect of different rotational speeds on the flow field

During the horizontal centrifugal casting process, the molten high temperature alloy undergoes circular motion. In the radial direction, an arbitrary interface is chosen, and the mass M on it is designated as the research object, as depicted in Fig. 7. Throughout the entire centrifugal casting process, the principal forces acting on this particle M consist of gravity, centrifugal force, Coriolis force, and frictional force. Among these forces, gravity and centrifugal force persist throughout the entire casting process [20]. The gravitational force remains constant, with G=Mg, and its direction is downward (the -Z direction). The equation for the centrifugal force is:

$$F_{ce} = MwR_c^2 \tag{6}$$

Where:

M …The quality of the selected points [kg];

w …The speed of the centrifuge [rad/s];

R_c …The radius of the particle from the center of the circle [m].

The Coriolis force and frictional force both arise from the relative motion of the molten high temperature alloy with respect to the bearing body. When the molten high temperature alloy is accelerated to the rated speed by the centrifugal force and a relatively stationary state is established, the Coriolis force and frictional force will correspondingly vanish. The expressions for the Coriolis force F_{co} and frictional force F_f are:

$$\begin{cases} F_{co} = 2Mwv \\ F_f = \mu F_{ce} \end{cases} \tag{7}$$

Based on the above mechanical analysis, it is evident that the acceleration of the molten high temperature alloy particle is the vector sum of the accelerations generated by the four forces. By resolving the acceleration of the molten high temperature alloy particles along the X axis, Y axis, and Z axis directions, the following equation can be derived.

$$\begin{cases} a_x = (1-\mu)\omega^2 x + 2\omega v_x \\ a_y = 0 \\ a_z = (1+\mu)\omega^2 z + 2\omega v_z - g \end{cases} \tag{8}$$

Where:

a_x, a_y, a_z …The components of acceleration in the x-axis, y-axis, and z-axis directions, respectively.

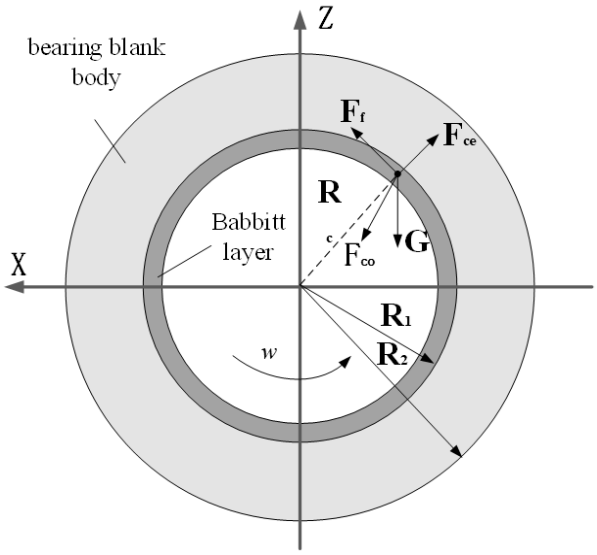

Fig. 7 *Force analysis of particles on the alloy layer*

To investigate the variation of the flow field under different centrifugal forces, under the condition that other initial conditions remain unchanged, the rotational speeds of the aforementioned simulation models were set at 280 r/min, 380 r/min, and 480 r/min, respectively. In the procast software, the "remove revolution velocity" function was adopted to obtain the velocity distribution of the flow field under different centrifugal forces as shown in Fig. 8. After removing the revolution velocity from the high-temperature liquid, its actual flow condition relative to the bearing blank body can be effectively demonstrated. As is clearly observable from Fig. 8, the molten high temperature alloy flows in the direction of rotation and diffuses towards the end faces on both sides. Its maximum velocity is essentially located at the edge position. The higher the centrifugal speed is, the faster the flow speed of the molten alloy of the superalloy will be; however, the increase in flow speed is not proportional to the centrifugal speed and the gap is very small. The above phenomenon is attributed to the fact that the initial velocity of the molten high-temperature alloy is determined by the frictional force. Additionally, it can be noted that the lower the flow velocity, the more likely the molten high temperature alloy is to accumulate in the middle area.

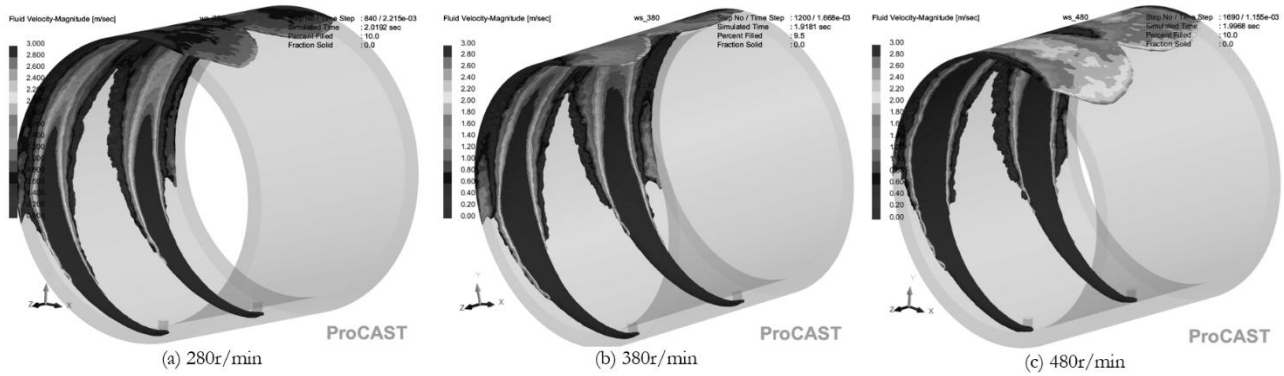

Fig. 8 *Flow field at different speeds (inlet radius 12 mm)*

In conclusion, it can be seen that the higher the centrifugal speed, the greater the centrifugal force exerted on the molten high-temperature alloy. However, the centrifugal force has a relatively small impact on the change in the shape of the flow field of the molten high-temperature alloy. Nevertheless, a large centrifugal force will lead to compositional segregation (such as heavy elements like tin and lead in Babbitt metal). Therefore, the centrifugal rotational speed needs to be further optimized.

5.3 Solidification process and analysis

As the filling process concludes, the centrifugal casting is on the verge of entering the solidification stage. This solidification process operates on the principle of heat transfer from the metal to the cooler mold or the surrounding environment [21, 22]. In the centrifugal casting model, the temperature of the bearing body is set at 300 °C, the temperature of the baffles on both sides is 30 °C, the end temperature of the centrifugal casting simulation is 180 °C, and the overall cooling approach involves water cooling on the outer surface of the bearing body. Different from the traditional centrifugal casting model, the bearing body has a thickness of 250 mm, while the alloy layer is only 15 mm thick, a nearly 15 fold difference. Under the condition of a large wall thickness, the laws governing the cooling process of the bearing alloy layer urgently need to be explored and explained in greater depth.

Fig. 9 illustrates the solidification process of the entire centrifugal casting model. Heat transfer mainly occurs through the bearing body and the side plates on both sides, as well as via the surrounding air and water cooling on the body's surface to reach the final temperature. During the water cooling process on the surface of the bearing blank, the surface temperature of the bearing blank drops to 30 °C within 20 seconds, yet most of the bearing blank still remains at 300 °C. It is clear that the temperature change of the molten high temperature alloy is consistent in the initial 100 second time phase. Owing to the large thickness of the bearing blank, the temperature inside the bearing blank also dropped to 300 °C after 500 seconds, and a U shaped temperature distribution is formed, extending from both sides and the outer part of the bearing blank to the inner part. As can be observed from Fig. 9 (1), the last filled area is situated in the middle region, which is approximately the same as the last cooled position in Fig. 9 (7), and it is also the area where a large number of shrinkage porosities appear subsequently. This further validates the necessity of achieving as uniform a filling as possible during the filling process. After 2400 seconds, the entire alloy layer cools down to below the set temperature, and the inner surface of the casting is uneven.

In the casting process, shrinkage porosities are common defects in centrifugal casting and are also crucial factors influencing the bonding strength of

bearing alloy layers. There are numerous methods for determining shrinkage porosities, such as the solidification time gradient, Niyama criterion, and solid phase ratio gradient [23]. For this purpose, the Niyama criterion in Procast software was employed to examine the porosity and pore distribution throughout the entire solidification process. As can be seen from Fig. 9 (8), defects such as shrinkage cavities and porosities occur in the middle of the entire alloy layer, among which the defects in the area of the final filling are the most severe.

Fig. 10 presents the actual centrifugal casting process of bearings in the enterprise. It is clearly observable that the inner surface of the bearing casting exhibits an uneven bulge, and there is a distinct shrinkage porosity adjacent to the inlet of the centrifugal casting. This finding is in accordance with the results of the simulation model.

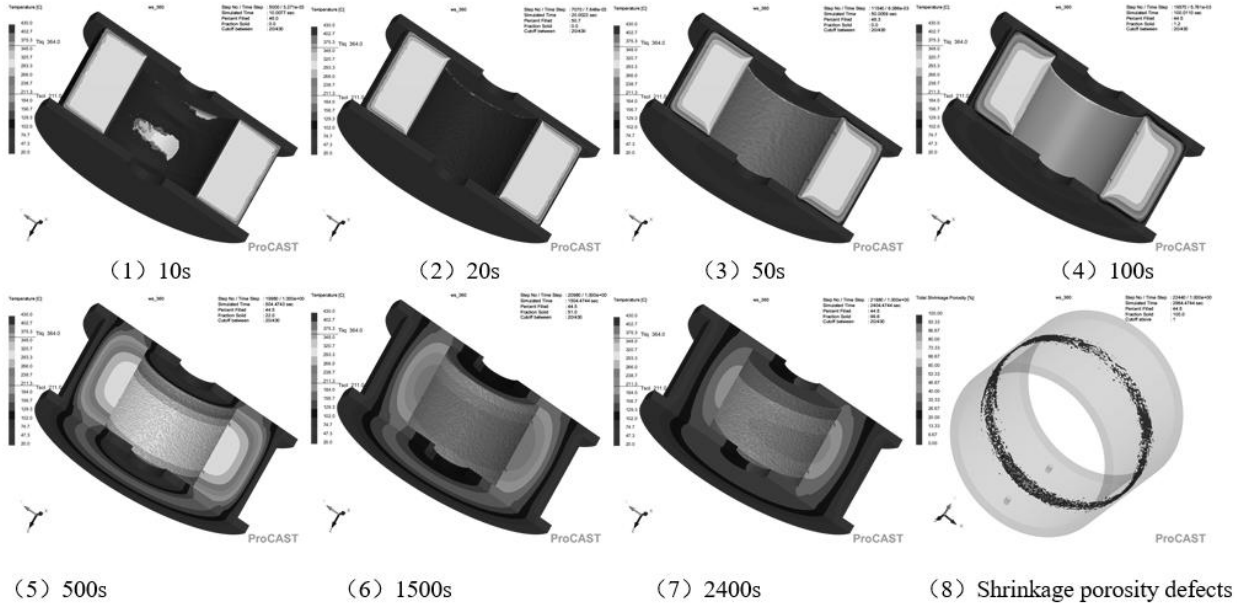

Fig. 9 *The solidification process of centrifugal casting patterns at different times*

Fig. 10 *Bearings after centrifugal casting*

6 Optimization and validation of process parameters

6.1 Orthogonal test protocol

Through the analysis of the filling and solidification processes of centrifugal casting, it becomes evident that the quality of the bearing alloy layer in centrifugal casting is mainly influenced by factors such as the casting temperature of Babbitt metal, the initial temperature of the bearing blank, the centrifugal speed, and the diameter of the filling inlet. As shown in Tables 2 and 3, based on the evaluation index of the shrinkage porosity volume, this study designed an orthogonal test scheme with 4 factors and 3 levels for the horizontal centrifugal casting of the alloy layer in a large wall thickness tilting pad bearing [24].

Tab. 2 *Factor level table*

Level	Initial temperature of Babbitt alloy (℃)	Initial temperature of bearing blank (℃)	Diameter of filling inlet (mm)	Centrifugal speed (r/min)
1	400	280	14	340
2	420	300	16	380
3	440	320	18	420

Based on the analysis results of the ProCAST orthogonal test, the sum of the test index values corresponding to each level K_i (i=1, 2, 3)and the influence amplitude R of the corresponding results for each factor were calculated, as presented in Tab.4. As is evident from Tab. 4, the influence of the initial temperature of the bearing blank and the centrifugation speed on the test results is significantly greater than that of other factors.

The optimal process parameters for horizontal centrifugal casting are as follows: the casting temperature of the Babbitt alloy is 440 °C, the initial temperature of the bearing blank is 280 °C, the diameter of the filling inlet is 16 mm, and the centrifugal rotational speed is 340 r/min. The results obtained from numerical simulation can provide certain assistance in formulating the centrifugal casting process scheme for the bearing. This is of great significance for the actual production of the enterprise as it can significantly reduce the number of experiments.

Tab. 3 *Orthogonal simulation experiment plan*

Factor scheme	Initial temperature of Babbitt alloy (℃)	Initial temperature of bearing blank (℃)	Diameter of filling inlet (mm)	Centrifugal speed (r/min)	Shrinkage porosity volume (cm^3)
1	400	280	14	340	45.245
2	400	300	16	380	50.336
3	400	320	18	420	56.501
4	420	280	16	420	50.132
5	420	300	18	340	46.882
6	420	320	14	380	56.017
7	440	280	18	380	47.806
8	440	300	14	420	54.20
9	440	320	16	340	48.948

Tab. 4 *Analysis of orthogonal simulation test results*

	Initial temperature of Babbitt alloy (℃)	Initial temperature of bearing blank (℃)	Diameter of filling inlet (mm)	Centrifugal speed (r/min)
K_1	152.082	143.183	155.462	141.075
K_2	153.031	151.418	149.416	154.159
K_3	150.954	161.466	151.189	160.833
R	0.692	6.094	2.015	6.586
Optimal level factor	3	1	2	1

6.2 Centrifugal Casting Verification

The process parameters for horizontal centrifugal casting derived from the ProCAST simulation described above were utilized to manufacture thrust bearing products on the centrifugal casting equipment of an enterprise in Zhuji City. Fig. 11 depicts a horizontal bearing alloy layer centrifugal casting product subsequent to the numerical simulation and machining processes. In accordance with the DL/T 297-2011 standard, the centrifugal casting was tested, and the processed internal surface was further examined. It was clearly ascertained that the castings were fully filled, with no apparent internal defects, and the finished product quality was excellent.

Fig. 12 presents the metallographic micrographs of the centrifugal casting. Despite the presence of rhombic hard dot segregation in the metallographic structure, its distribution is uniform, without aggregation. Although the density of the diamond shaped hard dot segregation in the metallographic structure inreases as it approaches the bottom, the overall distribution remains uniform and free of aggregation. As can be observed from the interface between the alloy layer and the iron base in Fig. 12 (a), the Babbitt layer and the iron base are well bonded, forming a distinct boundary. There are no obvious surface defects that could affect the bond strength, thus meeting the product quality requirements.

Fig. 11 *Thrust bearing products produced by Horizontal Centrifugal Casting*

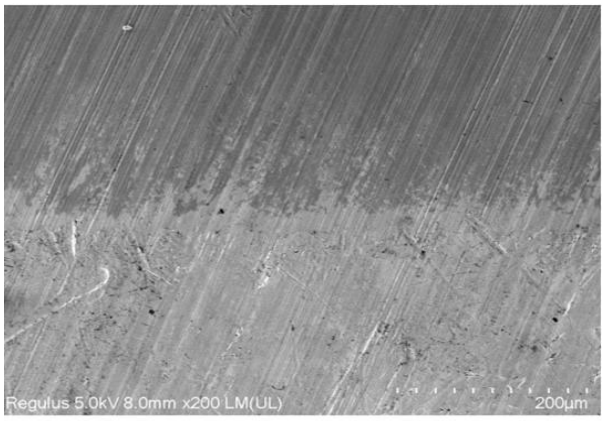

(a) Combine the interface

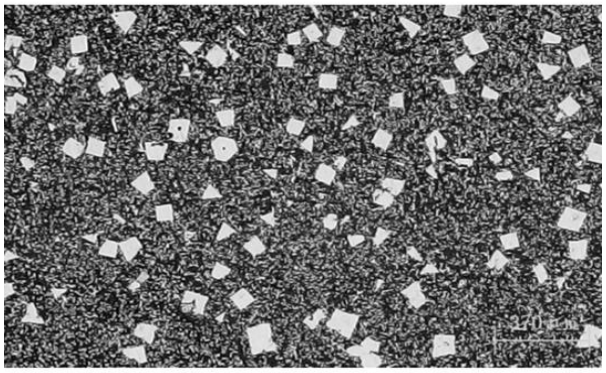

(b) Metallographic structure diagram

Fig. 12 *Bonding interface and metallographic diagram of alloy layer*

7 Conclusions

In this research, the influence mechanism of speed and filling time on the temperature and flow field of castings during the filling and solidification processes of large wall thickness centrifugal casting was investigated. A simulation model for large wall thickness centrifugal casting was constructed, and optimal process parameters were obtained via orthogonal tests, which were validated by the quality of actual castings. The following conclusions were drawn:

- (1) From the simulation of the gravity dominated stage, it was observed that the inlet area is approximately circular. When the inlet radius is too large (e.g., 12 mm), it expands the unfilled area in the middle. Conversely, when the inlet radius is too small (e.g., 6 mm), the molten high temperature alloy accumulates at the bottom. The centrifugal velocity has a relatively minor impact on the change in the flow field shape but exerts a significant influence on the segregation of the alloy composition.
- (2) During the cooling process of the bearing alloy layer, owing to the large wall thickness, the temperature distribution assumes a U shape. Even after 500 s, there are still certain areas within the bearing blank that have not reached 300 °C. Additionally, the last cooled area is located in the middle, which corresponds to the location of shrinkage cavities.
- (3) Through numerical models with different process parameters and orthogonal test simulations, the optimal process parameters were determined as follows: the casting temperature of the Babbitt alloy is 440 °C, the initial temperature of the bearing blank is 280 °C, the diameter of the filling inlet is 16 mm, and the centrifugal rotational speed is 340 r/min.

Acknowledgement

The work of this paper is supported by Zhejiang Province Visiting Engineering Project No. FG2024247.

References

[1] MAO, M., CHEN, J., XU, G., XIE, R., XIA, X. D., XU, Y. (2023). Bearing capacity calculations and experimental study on fluid pivot tilting pad journal bearings of hydraulic turbine. *Journal of Hydroelectric Engineering*, Vol. 42, No. 2, pp. 105-115.

[2] BADAWI, M. B., CROSBY, W. A, & ALKOMY, M. H. (2020). Performance analysis of tilting pad journal bearing using comsol multiphysics and neural networks. *AEJ Alexandria Engineering Journal*, Vol. 59, No. 2, pp. 865-881.dio 10.1016/j.aej.2020.03.015

[3] XUN, M. H., LUO, H. L., HAN, S. L, LI, S. P, ZHANG, L. (2023). Numerical Simulation and Application of Inclusion Movement in Horizontal Centrifugal Casting Pipe Filling Process. *Rare Metal Materials and Engineering*, Vol. 52, No. 7, pp. 2559-2564.

[4] JIANG, J. F., GE, N., & HUANG, D. C. (2023). Numerical simulation of squeeze casting of aluminum alloy flywheel housing with large wall thickness difference and complex shape. *Transactions of Nonferrous Metals Society of China*, Vol. 33, No. 5, pp. 1345-1360.

[5] XUN, M. H., LUO, H. L., &ZHANG, J. (2023). Numerical Simulation and Trial Production of Solidification Structure of L605 Centrifugal Cast Pipe [J]. *Special Casting & NonferrousAlloys*, Vol. 43, No. 6, pp. 800-804.

[6] RAN, X. (2024). Design of spiral runner for vertical centrifugal casting process of large annular titanium alloy castings. *Special Casting & NonferrousAlloys,* Vol. 53, No. 7, pp. 2049-2058.

[7] WANG, X., CHEN, R., & WANG, Q., WANG, S., SUN, Y., XIA, Y., ZHOU, G., LI, G. L., QU, Y. (2023). Influence of casting temperature and mold preheating temperature on centrifugal casting by numerical simulation. *Journal of Materials Engineering and Performance*, Vol. 32, No. 15, pp. 6786–6809.

[8] WANG, X., CHEN, R., WANG, Q., WANG, S., LI, Y., & XIA, Y., et al. (2022). Influence of rotation speed and filling time on centrifugal casting through numerical simulation. *International Journal of Metalcasting*, Vol. 17, No. 2, pp. 1326-1339.

[9] XIN, M., WANG, Z., LU, B., & LI, Y. (2022). Effects of different process parameters on microstructure evolution and mechanical properties of 2060 al–li alloy during vacuum centrifugal casting. *Journal of Materials Research and Technology*, Vol. 21, pp. 54-68.

[10] DONG, Q., YIN, Z., LI, H., GAO, G., & MAO, Y. . (2021). Simulation study on filling and solidification of horizontal centrifugal casting babbitt lining of bimetallic bearing. *International Journal of Metalcasting*, Vol. 15, No. 1, pp. 119-129.

[11] YANG, Y., WANG, X., LI, X., ZHOU, R., HE, Z., & JIANG, Y. (2024). Numerical simulation on solidification during vertical centrifugal casting process for TC4 alloy wheel hub with enhanced mechanical properties. *Materials*, Vol. 17, No. 1, pp. 187.

[12] YU-CHOL, K., NONG-I., P., & RIM-HYOK, B. G. (2024). Improvement of quality and yield for investment casting of centrifugal pump impeller by tilting mold and optimizing runner/riser system. The *International Journal of Advanced Manufacturing Technology*, Vol. 130, No. 5/6, pp. 2369-2379.

[13] MAZLOUM, K., NJJAR, A. A., & SATA A. (2024). Defect prediction and performance optimization of a413 vertical centrifugal castings through fea-based simulation. *Engineering Research Express*, Vol. 6, No. 3, pp. 035428.

[14] SHI K. (2022). Numerical simulation of mold filling and solidification process in centrifugal investment casting of complex thin-wall titanium alloy casting [D]. Huazhong University of Science and Technology.

[15] MOHAMED KARROUM, MARWA A. ABBAS, AHMED RAMADAN, MOHAMED A. GEPREEL. (2024). Effect of Normal Ageing in Bundle on the Mechanical Properties of Tempcore Treated Reinforcing Steel Rebar. *Manufacturing Technology*, Vol. 24, No. 5, pp. 779-790. DOI: 10.21062/mft.2024.088.

[16] LIU, L., CAO, Y., Ma, C., & Zhang, S. (2024). Coupling simulation and mechanism analysis of grain formation and growth in horizontal centrifugal casting. *International Journal of Metalcasting.* https://doi.org/10.1007/s40962-024-01470-x

[17] ZHAO, C., YANG, J., LI, M., et al. (2023). Effect on Surface Properties of H13 Mold Steel Cladding Layer by ScanningStrategy. *Advances in Manufacturing*, Vol. 23, No. 3, pp. 380-390. DOI: 10.21062/mft.2023.035.

[18] WANG, Y., QIN, F., QI, H., QI, H., & MENG, Z. (2022). Interfacial bonding behavior and mechanical properties of a bimetallic ring blank subjected to centrifugal casting process. *Journal of Materials Engineering and Performance*, Vol. 31, No. 4, pp. 3249–3261.

[19] WANG Yin, LI Yong, QIAN Xiao-ming, ZHANG Bo-si. (2022). Effect of the cooling rate of vacuum centrifugal casting on microstructure and mechanical properties of 7055 aluminum alloy. *Journal of Northeastern University(Natural Science)*, Vol. 43, No. 12, pp. 1769-1776.

[20] MCF A., MZ A., HC A. & UH B. (2020) Thermosolutal convection and macrosegregation during directional solidification of tial alloys in centrifugal casting. *International Journal of Heat and Mass Transfer*, Vol. 154, pp. 119698.

[21] LI, F., WANG, D., JIANG, Y., YANG, L., ZHAO, Y., & ZHANG, X. (2019). Effect of centrifugal casting process on mold filling and grain structure of K418B turbine guide. *The International Journal of Advanced Manufacturing Technology,* Vol. 104, No. 5-8, pp. 3065-3072.

[22] JIA, Y., QI, H., LI, Z., LIAN, X., PEI, M., ZHANG, H., & JIA, L. (2023). Influence of Pouring Temperature on Interfacial Bonding of 40Cr/Q345B Bimetallic Ring Blank Produced by Centrifugal Casting. *Journal of Materials Engineering and Performance*, Vol. 33, No. 7, pp. 3249-3261. https://doi.org/10.1007/s11665-023-08185-w.

[23] HE, Y., QIN, F., DENG, X., & WANG, Y. (2023). Study on Interface Bonding Behavior and Quality Control of 40Cr/Q345B Bimetallic Ring Blank in Vertical Centrifugal Casting. *Journal of Materials Engineering and Performance*, Vol. 33, No. 19, pp. 10310-10323.

[24] ZHAO, C., MA, C., et al. (2022). Analysis of the Effect of Preset Surface Texture on Hard State Cutting. *Manufacturing Technology*, Vol. 22, No. 3, pp. 384-394. DOI: 10.21062/mft.2022.034